medRxiv preprint doi: https://doi.org/10.1101/2022.03.31.22273226; this version posted March 31, 2022. The copyright holder for this preprint (which was not certified by peer review) is the author/funder, who has granted medRxiv a license to display the preprint in perpetuity. It is made available under a CC-BY-NC-ND 4.0 International license .

Cross-talk between red blood cells and plasma influences blood flow and omics phenotypes in severe COVID-19

Steffen M. Recktenwald[1,a,*], Greta Simionato[1,2,a,*], Marcelle G. M. Lopez[1,3], Fabia Gamboni[4], Monika Dzieciatkowska[4], Patrick Meybohm[5], Kai Zacharowski[6,7], Andreas von Knethen[6,7], Christian Wagner[1,8], Lars Kaestner[1,9], Angelo D'Alessandro[4], and Stephan Quint[1,3]

[1]Dynamics of Fluids, Department of Experimental Physics, Saarland University, Saarbrücken, Germany
[2]Institute for Clinical and Experimental Surgery, Campus University Hospital, Saarland University, Homburg, Germany
[3]Cysmic GmbH, Saarbruecken, Germany
[4]Department of Biochemistry and Molecular Genetics, University of Colorado Denver, Anschutz Medical Campus, Aurora, CO
[5]Department of Anesthesiology, Intensive Care, Emergency and Pain Medicine, University Hospital Wuerzburg, Wuerzburg, Germany
[6]Department of Anesthesiology, Intensive Care Medicine and Pain Therapy, University Hospital Frankfurt, Frankfurt, Germany
[7]Fraunhofer Institute for Translational Medicine and Pharmacology ITMP, Frankfurt, Germany
[8]Department of Physics and Materials Science, University of Luxembourg, Luxembourg City, Luxembourg
[9]Theoretical Medicine and Biosciences, Campus University Hospital, Saarland University, Homburg, Germany
[a]These authors contributed equally to this work.
[*]Correspondence: steffen.recktenwald@uni-saarland.de, greta.simionato@uni-saarland.de

ABSTRACT Coronavirus disease 2019 (COVID-19) is caused by the Severe Acute Respiratory Syndrome Coronavirus 2 (SARS-CoV-2) and can affect multiple organs, among which is the circulatory system. Inflammation and mortality risk markers were previously detected in COVID-19 plasma and red blood cells (RBCs) metabolic and proteomic profiles. Additionally, biophysical properties, such as deformability, were found to be changed during the infection. Based on such data, we aim to better characterize RBC functions in COVID-19. We evaluate the flow properties of RBCs in severe COVID-19 patients admitted to the intensive care unit by using *in vitro* microfluidic techniques and automated methods, including artificial neural networks, for an unbiased RBC analysis. We find strong flow and RBC shape impairment in COVID-19 samples and demonstrate that such changes are reversible upon suspension of COVID-19 RBCs in healthy plasma. Vice versa, healthy RBCs immediately resemble COVID-19 RBCs when suspended in COVID-19 plasma. Proteomics and metabolomics analyses allow us to detect the effect of plasma exchanges on both plasma and RBCs and demonstrate a new role of RBCs in maintaining plasma equilibria at the expense of their flow properties. Our findings provide a framework for further investigations of clinical relevance for therapies against COVID-19 and possibly other infectious diseases.

1 INTRODUCTION

Infection with the Severe Acute Respiratory Syndrome Coronavirus 2 (SARS-CoV-2) can lead to the development of the Coronavirus disease 2019 (COVID-19) (1). The pathophysiology of COVID-19 is characterized by respiratory manifestations but also involves increased inflammatory responses (2), alterations in the number and phenotype of blood cells (3, 4), microthrombotic complications, and vascular occlusions that can be fatal (5–7). In these changes, red blood cells (RBCs) were found to exhibit structural protein damage, membrane lipid remodeling (8), dysregulation in serum levels of coagulation factors (9), as well as altered physical and rheological properties, such as shape, size, and deformability (4, 10). Changes in RBC mechanical properties, such as its bending rigidity and cytoplasm viscosity, can dramatically alter their morphology, reduce microvascular perfusion, and impact flow behavior and hemorheology of blood in the circulatory system, eventually affecting gas transport efficiency (11–15). Such effects may play a role in COVID-19 severity. However, the origin of pathological changes of COVID-19 RBCs and their impact on blood flow remains poorly understood. RBC flow properties are particularly relevant in the microvasculature, especially in capillaries, where gas exchanges and microthrombotic events occur. Recently, Kubánková *et al.* (4) studied the microfluidic flow of RBCs from COVID-19 patients suspended a in phosphate-buffered saline (PBS) solution in a channel with a cross-section of $20 \times 20\,\mu m^2$, resulting in cell velocities up to $30\,cm\,s^{-1}$. At such high velocities, RBC deformability turned out to be heterogeneous, with most of the RBCs being strongly elongated in the flow direction but some exhibiting circular, less deformable shapes compared with healthy controls. In human capillaries, which have diameters similar to RBC size (about $10\,\mu m$), confined flows confer to RBCs characteristic shapes that depend on the cell velocity and the surrounding medium (16, 17). We previously used a microfluidic setup with channel dimensions similar to the

medRxiv preprint doi: https://doi.org/10.1101/2022.03.31.22273226; this version posted March 31, 2022. The copyright holder for this preprint (which was not certified by peer review) is the author/funder, who has granted medRxiv a license to display the preprint in perpetuity. It is made available under a CC-BY-NC-ND 4.0 International license .

RBC size and analyzed RBC shapes at high detail by means of artificial neural networks (18) in a velocity range that resembles microvascular *in vivo* flow. Flow properties of RBCs depend on biophysical cell features that are influenced by biochemical characteristics. In order to elucidate the effects of COVID-19 on RBCs, we study their shapes and flow properties in autologous and allogeneic plasma in similar confined microfluidic channels in comparison to healthy controls. We observe RBC flow impairment in COVID-19 plasma and a full recovery upon suspension in healthy plasma. To better elucidate these effects, we additionally characterize both RBC and plasma content by proteomics and metabolomics analysis, highlighting a mutual influence of RBC and plasma and discovering a new role of RBC in establishing plasma equilibria in COVID-19.

2 MATERIALS AND METHODS

2.1 Blood collection

Nine mL of blood is drawn in heparin tubes from five healthy volunteers under informed consent and 14 COVID-19 patients admitted at the Intensive Care Unit (ICU) at the Frankfurt University Hospital, seven of which with supported ventilation and six receiving extracorporeal membrane oxygenation (ECMO) (Online Supplementary Table S1). The study is performed according to the Declaration of Helsinki and under the approval of the Fraunhofer Institute for Translational Medicine and Pharmacology ethics committee (reference #20-643, #20-982). Healthy and patient blood tubes are transported at room temperature and processed after 2 hours from blood drawing.

2.2 Sample preparation

Blood is leukodepleted (Pall's Acrodisc PSF syringe filters, Pall Corporation, New York, NY) and centrifuged at $1500 \times g$ for 5 minutes to separate RBCs and plasma. RBCs are then suspended in PBS (Gibco PBS, Thermo Fisher, Bremen, Germany) and the centrifugation and washing steps are repeated three times. Plasma fraction is centrifuged at $5000 \times g$ for 5 minutes to assure the removal of platelets, then used to resuspend washed RBCs in autologous plasma at a final hematocrit of 0.5 %. Additionally, patient RBCs are suspended in blood group-matching control plasma and control RBCs in patient plasma. Hence, we obtain four sample groups; (i) control RBCs in control plasma (CinC), (ii) patient RBCs in patient plasma (PinP), (iii) control RBCs in patient plasma (CinP), and (iv) patient RBCs in control plasma (PinC) (Figure 1A).

2.3 Microfluidic setup

A microfluidic channel with a rectangular cross-section of 8 µm height (H) and 11 µm width (W) (Figure 1B) is used to pump RBC suspensions as described (17). RBC flow x-y-plane is recorded with a frame rate of up to 400 fps using a pressure drop range between 100 mbar and 1000 mbar. The resulting cell velocities are in the range of $0.1\,\mathrm{mm\,s^{-1}}$ and $7\,\mathrm{mm\,s^{-1}}$, similar to the flow in the microvascular network (19, 20).

2.4 Flow analysis

Velocity, lateral cell position in the y-direction, and projection area of each cell are determined using a customized python script. Based on RBC velocity, the distribution of RBC lateral y-position is used as a characteristic indicator of the single-cell flow in such confined microchannels (16–18). The difference between pathological and healthy single-cell flow behavior is quantified by the so-called y-deviation, which relates the y-distribution of a given sample to the average distribution for healthy controls at specific cell velocities (Online Supplementary Figure S1). Additionally, we use a convolutional neural network to classify RBC shapes, as previously described (18).

2.5 OMICS sample collection

Four hundred µL packed RBCs is suspended in 1 mL autologous or allogeneic compatible plasma for 20 minutes at 4°C. Plasma is collected according to a modified Folch extraction method (21) and the three fractions obtained (lipid, metabolite and protein-enriched) are stored in liquid nitrogen until analysis, as well as packed RBCs after suspension in autologous or allogeneic plasma. Samples are collected from three healthy controls and eight patients, of which four were with supported ventilation and four on ECMO.

2.6 Ultra-High-Pressure Liquid Chromatography-Mass Spectrometry (UHPLC-MS) metabolomics

A volume of 50 µL of frozen RBC aliquots is extracted in 950 µL methanol:acetonitrile:water (5:3:2, v/v/v). Samples are vortexed and insoluble material pelleted as described (22). Analyses are performed using a Vanquish UHPLC coupled online to a Q Exactive mass spectrometer (Thermo Fisher, Bremen, Germany). Samples are analyzed using a 3-minute isocratic condition or a 5, 9, and 17 minutes gradient as described (23). Solvents are supplemented with 0.1 % formic acid for positive mode runs and 1 mM ammonium acetate for negative mode runs. MS acquisition, data analysis, and elaboration are performed as described (23). Additional analyses, including untargeted analyses and Fish score calculation via MS/MS, are calculated against the ChemSpider database with Compound Discoverer 2.0 (Thermo Fisher, Bremen, Germany).

2.7 Proteomics

Proteomics analyses are performed via filter aided sample preparation (FASP) digestion and nano UHPLC-MS/MS identification (TIMS TOF Pro 2 Single Cell Proteomics, Bruker Daltonics, Bremen, Germany), as previously described (24).

medRxiv preprint doi: https://doi.org/10.1101/2022.03.31.22273226; this version posted March 31, 2022. The copyright holder for this preprint (which was not certified by peer review) is the author/funder, who has granted medRxiv a license to display the preprint in perpetuity. It is made available under a CC-BY-NC-ND 4.0 International license .

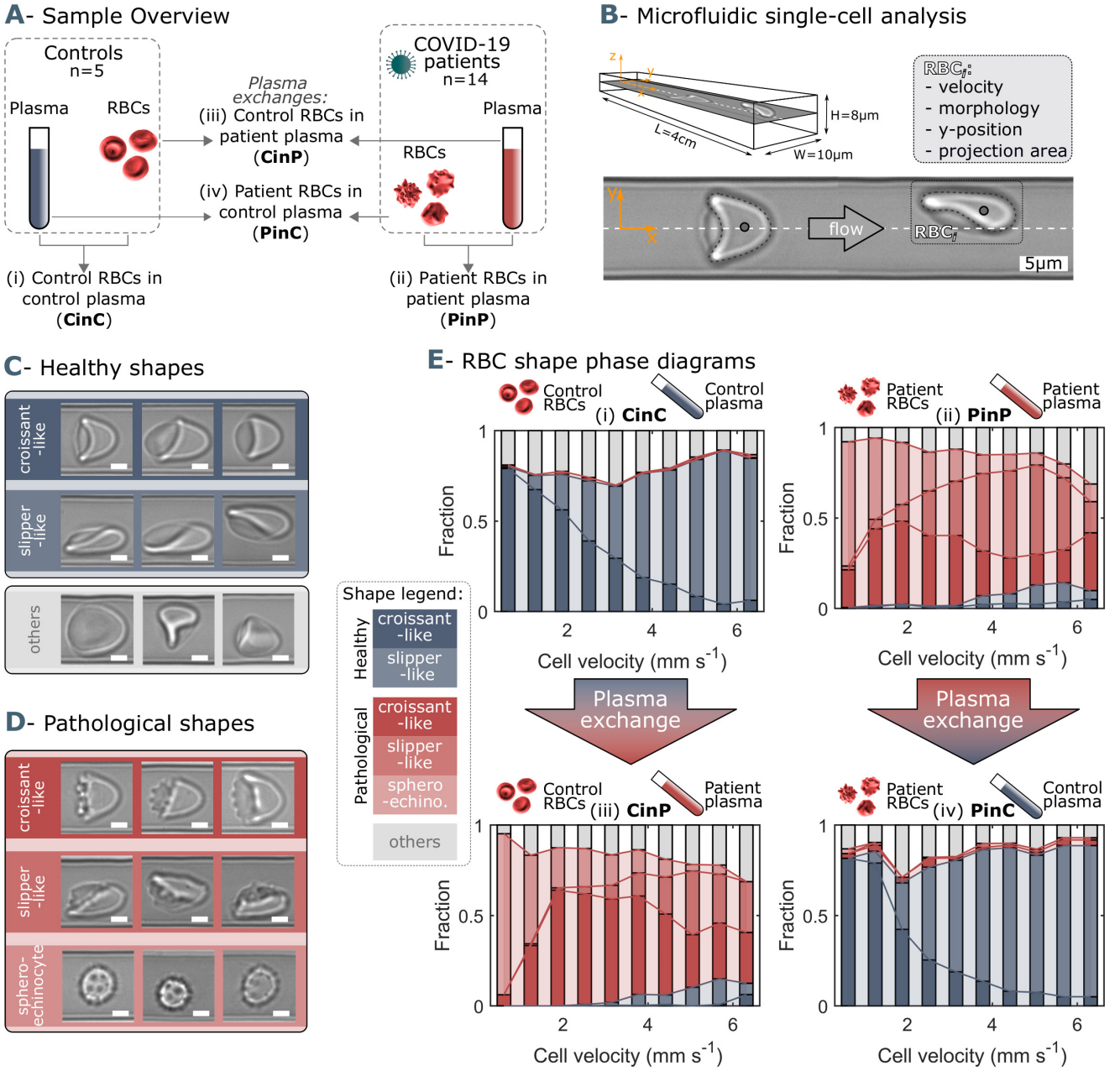

Figure 1: **Microfluidic setup, representative red blood cell (RBC) shapes in healthy and COVID-19 patients and related phase diagrams.** (A) Overview of the four sample groups, referred to as "X RBCs in X plasma", e.g. CinC for Control RBCs in Control plasma, and so on for PinP, PinC, and CinP. (B) Schematic representation of microfluidic channel dimensions and analysis method. Representative images of (C) healthy and (D) pathological RBC shapes found in COVID-19 patients. Scale bars in (C) and (D) correspond to a length of 2.5 µm. (E) Representative shape phase diagrams of two donors (a control and a patient) for the four sample groups. The upper panels show the phase diagram of the donors in autologous plasma, while the lower panels correspond to the same donors in allogeneic exchanged plasma.

2.8 Statistical analyses

Graphical representations and statistical analyses by T-test, repeated measures ANOVA or Kruskal-Wallis test are performed with GraphPad Prism (GraphPad Software, Inc, La Jolla, CA), MATLAB (MathWorks, Natick, MA), and MetaboAnalyst 5.0. Spearman's rank correlation coefficient analysis is applied between the microfluidic and omics data. Both correlation data and omics raw data are included in Online Supplementary Table S2.

medRxiv preprint doi: https://doi.org/10.1101/2022.03.31.22273226; this version posted March 31, 2022. The copyright holder for this preprint (which was not certified by peer review) is the author/funder, who has granted medRxiv a license to display the preprint in perpetuity. It is made available under a CC-BY-NC-ND 4.0 International license .

3 RESULTS

3.1 COVID-19 patients exhibit pathological changes of RBC shapes in capillary flow

In confined flows with dimensions on the same order of magnitude as the diameter of RBCs, healthy RBCs predominantly deform into the centered croissants and off-centered slipper shapes (Figure 1C), depending on the cell velocity. RBCs of COVID-19 patients additionally exhibit complementary pathological croissant and slipper shapes that resemble their corresponding healthy classes but display pronounced spicules on the membrane (Figure 1D). Further, COVID-19 patients show sphero-echinocytes in flow, known as irreversible transformations of RBCs that can occur upon ATP depletion, high pH, or exposure to anionic detergents (25, 26) (Figure 1D). The so-called RBC shape phase diagram (16–18) describes the frequency of occurrence for RBC morphologies as a function of cell velocity. While croissant- and slipper-like shapes emerge for control samples in autologous plasma (CinC), corresponding pathological shapes and sphero-echinocytes dominate for patient RBCs in autologous plasma (PinP) (Figure 1E, top graphs). This initial assessment highlights the dramatic shape difference between control and COVID-19 patient RBCs. However, upon plasma exchange with healthy control plasma, patient RBCs (PinC) show an immediate shape reversal, exhibiting a phase diagram similar to healthy controls. In contrast, control RBCs in allogeneic exchanged COVID-19 plasma (CinP) result in a drastic RBC shape deterioration (Figure 1E, bottom graphs). Besides these results in microcapillary flow, sphero-echinocytes for COVID-19 patients in autologous plasma (PinP) are also found in stasis and highlight impaired RBC clustering (Online Supplementary Figure S2, A). However, upon plasma exchange (PinC), RBC shapes in stasis revert to biconcave disks and are able to aggregate into rouleaux. The opposite trend is observed for control cells suspended in patient plasma (CinP) (Online Supplementary Figure S2, B).

The so-called shape ratio, which relates the number of pathologically shaped cells (Figure 1D) to the number of healthy cells (Figure 1C), quantifies the extent of pathological RBC shape changes. While the shape ratio is considerably smaller than one for healthy controls (CinC), COVID-19 patients (PinP) show shape ratios two orders of magnitude higher in autologous plasma (Figure 2A). Upon plasma exchange (PinC), all patients exhibit a decrease in the shape ratio, hence a reduction in the number of pathological RBC shapes. In contrast, healthy RBCs suspended in COVID-19 plasma (CinP) show an increase in the shape ratio between two to four orders of magnitude compared to their control condition (CinC). Similarly, suspension in allogeneic plasma results in a reduction of sphero-echinocytes for all patients, while an increase is observed for all controls in COVID-19 plasma (Figure 2B). The pronounced number of sphero-echinocytes in RBCs suspended in COVID-19 plasma leads to a decrease of the 2D projection area in the x-y-plane compared to healthy shapes (Figure 2C). The large number of sphero-echinocytes and the impaired deformability of pathological RBCs in COVID-19 plasma (PinP and CinP) hinders the formation of stable slipper-shaped RBCs at high velocities. This causes pronounced deviations from the single-cell flow behavior of healthy cells, as expressed by the deviation in the equilibrium position in y-direction (Figure 2D).

3.2 Multiomics analyses reveal a tight interaction between plasma and RBCs

To delve into the molecular underpinnings of RBC shape changes in COVID-19 and the reversal of such phenomenon upon incubation with healthy control plasma we perform multiomics analysis, including proteomics and metabolomics, of the four sample groups (CinC, PinP, PinC, and CinP). RBCs and plasma from all four conditions are examined separately.

3.2.1 RBCs affect plasma content

The comparison between control (CinC) and patient (PinP) plasma shows two clusters of differentially abundant proteins and metabolites (Figure 3A). Control plasma content results in higher levels of albumin (ALB), transferrin (TF), and gelsolin (GSN). Decreased levels of such proteins are associated with hypercoagulability, higher inflammatory state, and severity in COVID-19, respectively (28–30). On the contrary, patient plasma is associated with an increase in inflammation and coagulation markers, such as complement cascade proteins (such as C2, C3, C5, C7, C9), SERPINA1, SERPINA3, and SERPINA G1 and C-reactive protein (CRP).

After placing RBCs of patients in control plasma (PinC) and vice versa control RBCs in patient plasma (CinP), plasma contents immediately change, influenced by RBCs. Specifically, the patient plasma becomes comparable to control plasma content upon suspension with control RBCs (CinP), while the opposite effect occurs in control plasma suspended with patient RBCs (PinC) (Figure 3A). This shows a strong influence of RBCs on plasma content and highlights the establishment of an equilibrium between RBCs and plasma. Notably, RBC shape ratio and sphero-echinocyte percentage are comparable in RBCs suspended in patient plasma, although plasma content is different. This means that RBC influence on plasma content occurs at the expense of RBC morphology, which, in turn, affects RBC flow properties. Additionally, these results show that the impairment of RBC shape is not directly caused by a specific plasma component but may derive from a complex interaction between plasma and RBCs. In agreement with the data in the heat map, principal component analysis (PCA) highlights four distinct groups, showing that plasma contents of the groups CinP and CinC result in neighboring clusters, while PinC and PinP clusters strongly overlap (Figure 3B).

Within the identified significantly different molecules in plasma (Figure 3A heatmap and Online Supplementary Table

medRxiv preprint doi: https://doi.org/10.1101/2022.03.31.22273226; this version posted March 31, 2022. The copyright holder for this preprint (which was not certified by peer review) is the author/funder, who has granted medRxiv a license to display the preprint in perpetuity. It is made available under a CC-BY-NC-ND 4.0 International license .

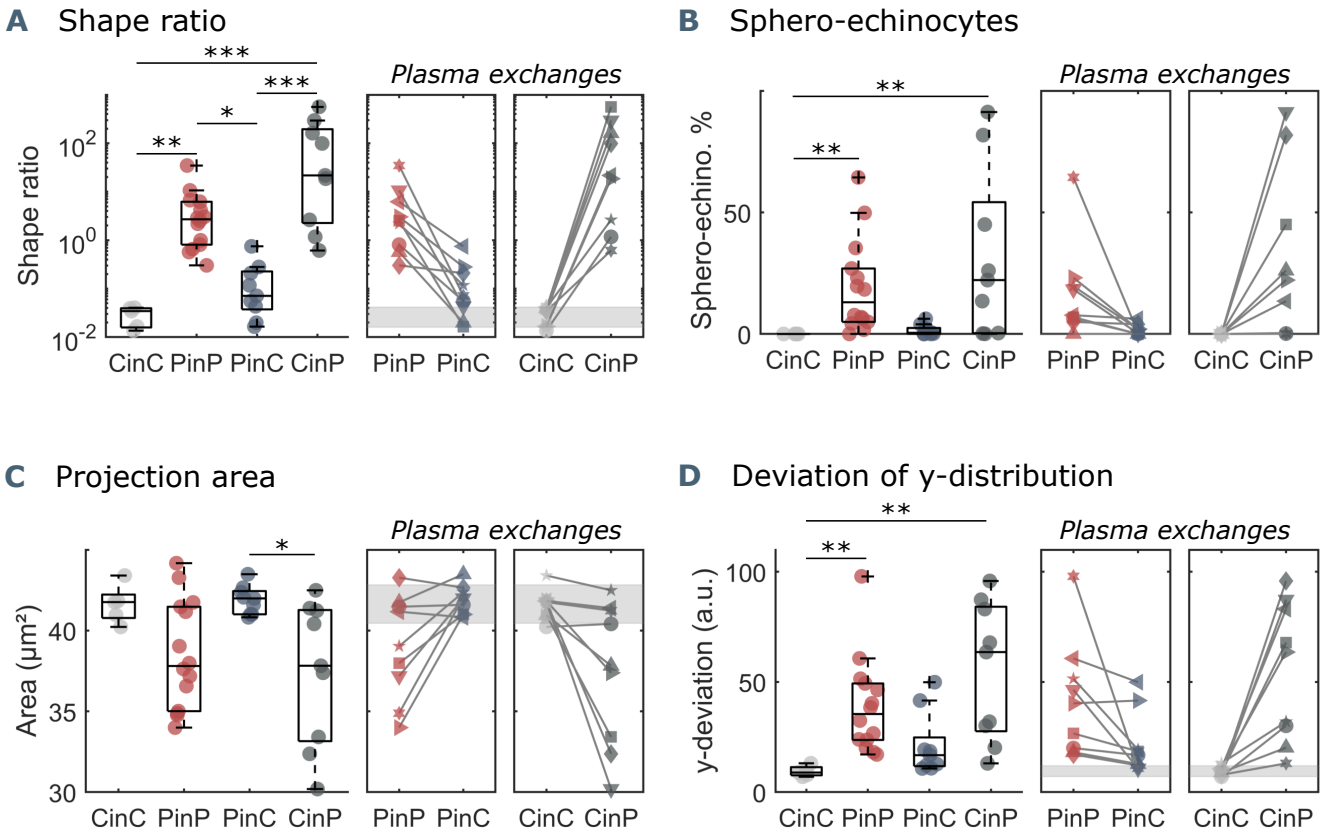

Figure 2: **Parameters used for microfluidic flow analysis for the four sample groups.** (A) Shape ratio, *i.e.*, the proportion of pathological to healthy RBC shapes, (B) percentage of sphero-echinocytes, (C) RBC 2D projection area in a velocity range of $1-3\,\mathrm{mm\,s^{-1}}$, and (D) deviation of the RBC distribution in y-direction based on the average of controls (CinC) in a velocity range of $5-10\,\mathrm{mm\,s^{-1}}$. Left panels (A-D) show data as boxplots with superimposed individual data points. The bottom and top of each box are the 25th and 75th percentiles of the sample, respectively. The line in the middle of each box is the sample median. Whiskers go from the end of the interquartile range to the furthest observation. Data beyond the whisker length are marked as outliers with '+' signs. * refers to a significance level of $p < 0.05$, ** to $p < 0.01$, and *** to $p < 0.001$. Right panels (A-D) show the effect of plasma exchange for individual donors. Gray areas correspond to the mean and standard deviations for controls (CinC) of the corresponding data.

S2) tryptophan metabolites deserve consideration. As previously described (31), tryptophan metabolism is altered in COVID-19 plasma, resulting in decreased anthranilate and indole acetaldehyde and increased kynurenine in patients, which is associated with a higher mortality risk (31, 32) (Figure 3C). Compared to control conditions (CinC), plasma kynurenine significantly increases upon exposure of patient RBCs in control plasma (PinC). Tryptophan levels are significantly lower in patient plasma (PinP) compared to controls (CinC), while they significantly increase for control RBCs in patient plasma (CinP). Plasma anthranilate levels and tryptophan/kynurenine (Trp/Kyn) ratio significantly differ in the groups with control RBCs (CinC and CinP) compared to patients groups (PinC and PinP). These data suggest a role of RBCs in buffering kynurenine content and related metabolites, thus potentially protecting from an increased risk for mortality in COVID-19 patients (Figure 3D).

3.2.2 RBC content is affected by plasma

Omics analyses on RBCs from each group reveal a cluster of proteins and metabolites that is comparable between CinC and PinP. Most of them involve plasma proteins, such as albumin (ALB), fibrinogen (FGA and FGB), gelsolin (GSN), transferrin (TF), serpins (SERPINA1, SEPRINC1), and immunoglobulin variables (IGHV439, IGHG2, IGKC) (Figure 4A), which instead result significantly different in the respective control and patient plasma samples.

Additionally, two clusters indicate that some characteristics of RBCs are maintained only when they are suspended in autologous plasma. Control RBCs (CinC) show higher levels of pantothenol, which is known to have antiseptic properties (33), adenosine and hydroxyglutarate that were found decreased in hypoxia (34), and formyl-kynurenine, probably buffering plasma kynurenine (Figure 4A). In contrast, the most abundant proteins in patient RBCs (PinP) are linked

medRxiv preprint doi: https://doi.org/10.1101/2022.03.31.22273226; this version posted March 31, 2022. The copyright holder for this preprint (which was not certified by peer review) is the author/funder, who has granted medRxiv a license to display the preprint in perpetuity. It is made available under a CC-BY-NC-ND 4.0 International license .

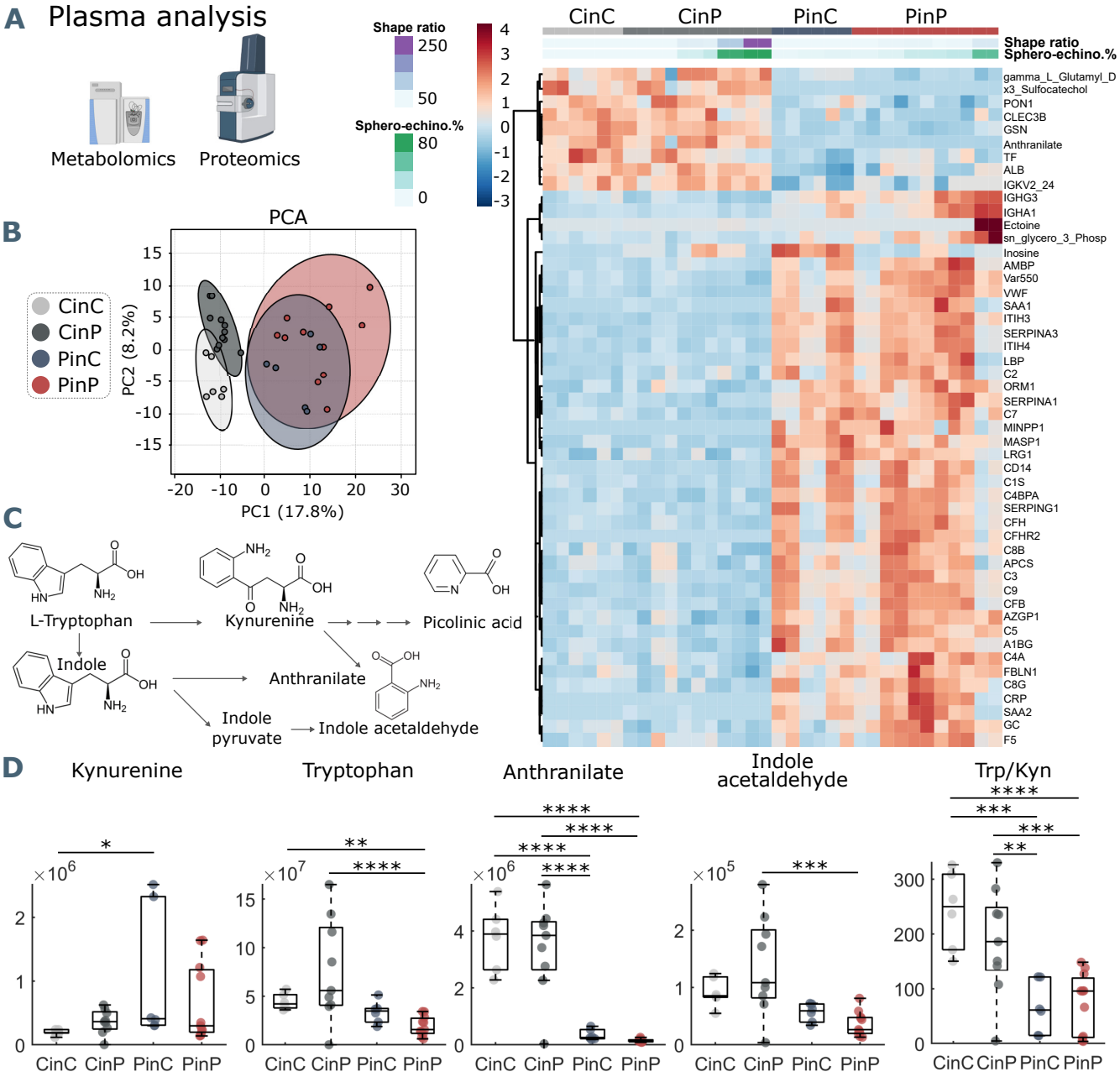

Figure 3: **Metabolomics and proteomics analyses of plasma from the four sample groups.** (A) Hierarchical clustering analysis of the top 50 metabolites and proteins by two-way ANOVA test. (B) Principal component analysis (PCA) shows distinct groups. (C) Schematic representation of tryptophan pathway to kynurenine, anthranilate, and indole acetaldehyde formation. (D) Boxplots of all samples for each group showing statistical differences in selected molecules generated in the tryptophan-kynurenine pathway. Y-axis indicates peak areas for each selected analyte, as determined by UHPLC-MS. Statistically-significant differences exist between controls (CinC) and patients (PinP) in the levels of tryptophan and anthranilate. Plasma exchanges cause strong significant differences in anthranilate levels and the ratio tryptophan-kynurenine (Trp/Kyn) in all groups, a marker of COVID-19 disease severity and mortality in previous studies (27).

to cellular responses to stress (Online Supplementary Figure S3), involving ubiquitination and protein degradation by the proteasome, which may be related to higher oxidative stress. Increasing levels of guanidinoacetate, ornithine, urate, and L-citrulline indicate higher catabolism of arginine.

Since RBCs influence plasma metabolites and protein abundance, they must necessarily adopt their metabolic and protein content. Indeed, an effect occurs when RBCs are

medRxiv preprint doi: https://doi.org/10.1101/2022.03.31.22273226; this version posted March 31, 2022. The copyright holder for this preprint (which was not certified by peer review) is the author/funder, who has granted medRxiv a license to display the preprint in perpetuity. It is made available under a CC-BY-NC-ND 4.0 International license .

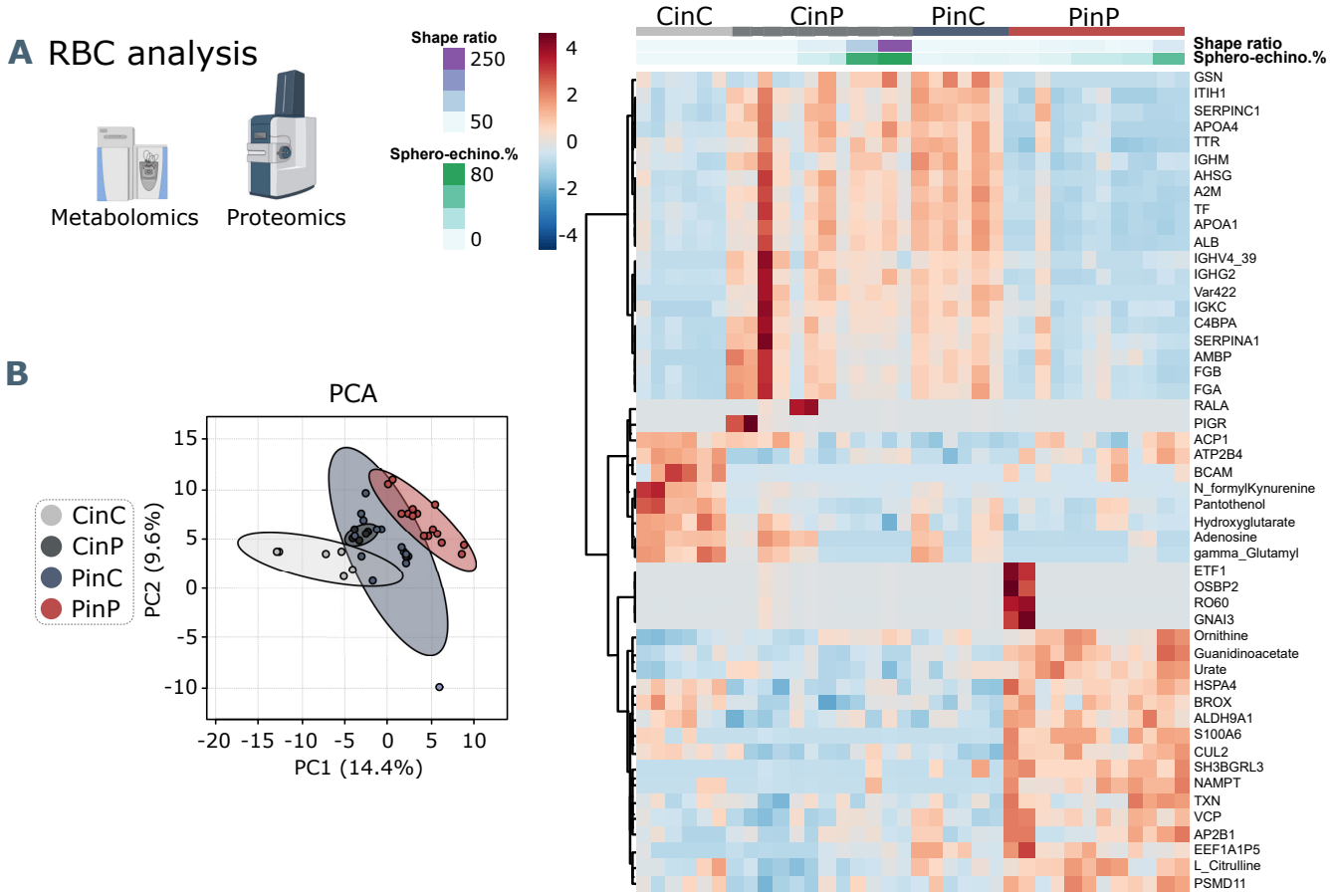

Figure 4: **Metabolomics and proteomics analysis on RBCs of the four sample groups.** (A) Hierarchical clustering analysis of the top 50 metabolites and proteins in RBCs by two-way ANOVA test. (B) PCA analysis from RBC content shows clusters of each sample group, where CinC is neighboured by the overlapping clusters CinP and PinC, and PinP as the furthest cluster.

suspended in allogeneic plasma (CinP and PinC), resulting in changed levels of plasma proteins (ALB, FGA, FGB, GSN, TF, SERPINA1, SEPRINC1) and immunoglobulin variables (IGHV439, IGHG2, IGKC) (Figure 4A). These data indicate RBC's ability to equilibrate their protein levels when coming in contact with the new plasma, since the first cluster is comparable between CinC and PinP and between CinP and PinC. However, the changes in RBC metabolism and protein content that occur upon suspension with allogeneic plasma do not reflect RBC morphological changes, since PinP samples exhibit many more pathological RBC shapes than PinC samples.

3.3 Pathological RBC shapes are associated with markers of inflammation, oxidation, and hypoxia

3.3.1 RBC morphological correlations with plasma components

The main plasma components correlating with sphero-echino cytes are lactate and 2,3-diphosphoglycerate (2,3-DPG), associated to increased glycolysis; nicotinamide and tryptophanamide, related to tryptophan metabolism; glutamate, creatine, and hypoxanthine, which was found to be positively correlated with creatinine (31); lactoferrin (LTF), an iron-binding protein with antimicrobial and anti-inflammatory activity (35); ectoine a compound associated to anti-inflammatory properties (36) and found in COVID-19 sera, as well as 2-oxoglutarate (also known as α-ketoglutarate) (37). The shape ratio also correlates to hypoxanthine, ectoine, and nicotinamide. TF levels negatively correlate to sphero-echinocyte percentage and shape ratio. TF was previously reported to decrease during COVID-19 infection (29). Similarly, the levels of arginine and tyrosine were previously reported to negatively correlate with disease severity, as gleaned by the levels of the inflammatory cytokine interleukin-6 (IL-6) (31). Analogously, decreases are observed in the levels of sulfur-containing amino acids, thiocysteine, 3-sufinoalanine, and cystine, a marker of redox homeostasis.

medRxiv preprint doi: https://doi.org/10.1101/2022.03.31.22273226; this version posted March 31, 2022. The copyright holder for this preprint (which was not certified by peer review) is the author/funder, who has granted medRxiv a license to display the preprint in perpetuity. It is made available under a CC-BY-NC-ND 4.0 International license .

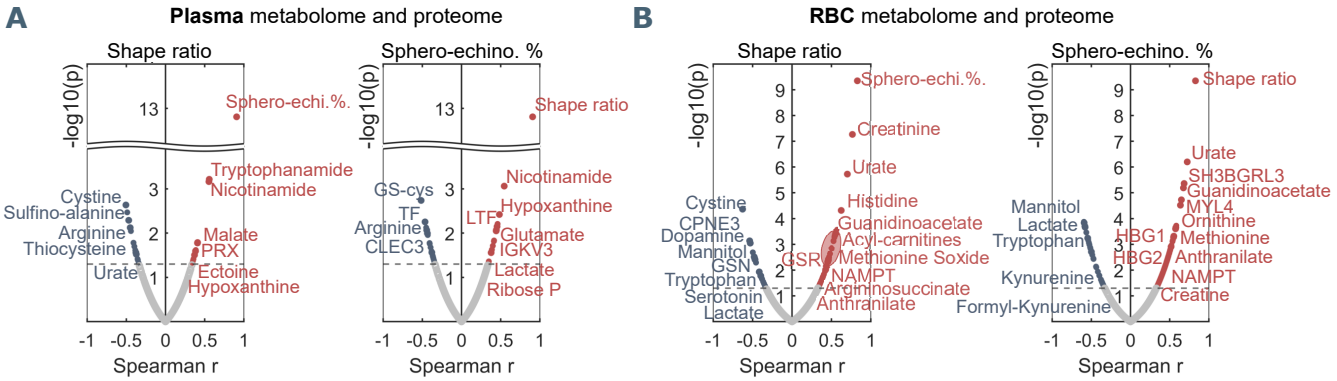

Figure 5: **Plasma and RBC Spearman correlation analysis of RBC shape parameters with omics data.** Volcano plot representations highlight the most significant proteins and metabolites in plasma (A) and in RBCs (B) positively (red) or negatively (blue) correlated to shape ratio (left panels in A and B) or sphero-echinocyte percentage (right panels in A and B). P values are plotted on the y-axis versus magnitude of change (fold change) on the X-axis; significance threshold is set at $p < 0.05$.

3.3.2 RBC morphological correlations with RBC content

Most correlations to both sphero-echinocytes and shape ratio are observed with respect to RBC content (Figure 5B, Online Supplementary Table S2). Negative correlations result with lactate, in contrast with the positive correlation in plasma, and mannitol, for which decreased levels are associated with reduced deformability of RBCs (38). Among the proteins is ALB, known to re-establish RBC discocyte shape in stored blood (39), TF, which is reduced in COVID-19 plasma and is correlated with increased levels of CRP and IL-6 ((29), Online Supplementary Table S2). Tryptophan and the related metabolites formyl-kynurenine, kynurenine and serotonin negatively correlate with pathological RBC shapes, coherently with lower levels seen in patient RBCs (formyl-kynurenine, Figure 4A). Serotonin and dopamine result negatively correlated with shape ratio. In contrast, positive correlations exist with several amino acids, such as methionine, tyrosine, lysine, histidine, threonine, and arginine catabolism products through the urea cycle, specifically citrulline, ornithine, arginine-succinate and urate. Creatine and creatinine levels also result positively correlated, further suggesting enhanced arginine catabolism. These results highlight that RBC buffering activity to contrast the altered amino acid metabolism implies their morphological impairment. Finally, while formyl-kynurenine and kynurenine negatively correlate, positive correlations exist with anthranilate and picolinic acid, suggesting the ability of pathological RBCs to buffer the kynurenine pathway metabolites. Positively correlated proteins are linked to different biological processes. Gas and ion transport-related proteins, such as carbonic anhydrase (CA2) and band3 (SLC4A1) are linked to pathological RBC shapes; a special highlight is a correlation with the expression of hemoglobin F subunits (HBG1 and HBG2). These data suggest a need to adjust oxygen transport, transporter activity, and pH buffering (chloride/bicarbonate ratios impact intracellular pH of RBCs) during the infection state (34). Other correlations are found with several proteasome-linked proteins, such as PSMB2, PSMB6, PSMA1, PSMC4, PSMC2 (Online Supplementary Figure S4) with an ATP-dependent function, indicating high levels of protein degradation and regulation of amino acid metabolism in pathological RBCs. Indications of an enhanced antioxidant activity to cope with increased oxidative stress in such cells is highlighted by positive correlations with glutathione metabolism-related enzymes, such as glutathione S-transferase Mu 3 (GSTM3), glutathione reductase (GSR), which maintains reduced glutathione, and glucose-6-phosphate dehydrogenase (G6PD), the rate-limiting enzyme for the pentose-phosphate pathway (PPP), which is the only source for NADPH generation in RBCs, thus the main pathway for protection against oxidative stress. In addition, a positive correlation exists with peroxiredoxin 1 (PRDX1) that catalyzes the reduction of hydrogen peroxide. Further correlations are found with nicotinamide-phosphoribosyl transferase (NAMPT), which catalyzes the biosynthesis of NAD, and NADH-cytochrome b5 reductase 3 (CYB5R3), which reduces methemoglobin, the oxidated form of hemoglobin to the ferric state.

Together, these data show that morphological impairments observed in RBCs flowing in COVID-19 patient plasma are strongly related to markers of inflammation, oxidation, and hypoxia, which are associated with increased mortality risk (27).

4 DISCUSSION

Our microfluidic analysis demonstrates a significantly increased number of pathological RBC shapes, such as sphero-echinocytes in the capillary flow of COVID-19 patients (PinP) (Figure 2A-C). These changes lead to an alteration of the microscale flow behavior since these RBCs are not able to adapt their shape to the imposed flow conditions compared to healthy controls (Figure 2D). Static images of the same suspensions confirm such morphological changes, where impaired RBCs can be visualized as sphero-echinocytes. These

medRxiv preprint doi: https://doi.org/10.1101/2022.03.31.22273226; this version posted March 31, 2022. The copyright holder for this preprint (which was not certified by peer review) is the author/funder, who has granted medRxiv a license to display the preprint in perpetuity. It is made available under a CC-BY-NC-ND 4.0 International license .

shapes do not aggregate into rouleaux but cluster into disorganized structures. However, RBCs are able to revert their shape to biconcave disks in stasis and healthy croissant and slipper shapes in flow, resulting in a single-cell flow behavior comparable to control samples. Interestingly, the reversibility of sphero-echinocytes contradicts previous literature. Up to now, it was assumed that sphero-echinocytes cannot reverse to discocytes due to membrane loss through vesiculation that imbalances the structure of the lipid bilayer (25). However, the shapes observed here must not involve such types of changes. Of note, echinocytes presence is not a specific feature of COVID-19 infection, but has been previously observed in stasis in blood smears of septic patients (40).

Patient plasma results in increased levels of inflammation and hypercoagulation markers, in accordance with previously published data (31). Particularly interesting due to its association with higher mortality risk is kynurenine, which decreases upon suspension of healthy control RBCs in COVID-19 plasma. Kynurenine levels are associated with hypoxia markers and interferon signaling (IFNG) (27, 41). The restoration of proteins and metabolites levels is acute and immediate and occurs at the expense of RBC shapes. These results highlight a non-previously identified "sponge-like" behavior of RBCs that rebalance plasma content. These influences and adaptations to the surrounding environment may be a specific feature of RBCs since they cannot synthesize new proteins and thus respond to needs through metabolic adjustments that also involve shape transformations. Proteomics and metabolomics data on RBCs indeed confirm that the differences between healthy and patient cells reflect the differences observed in their plasma content. A deeper investigation on morphologically impaired COVID-19 RBCs by correlation analysis results in their association with markers of inflammation, oxidation, and hypoxia in the plasma, features that act in a tight relation to overcome the infection.

Guanidinoacetate and ornithine correlations in patient RBCs suggest more activity of arginase that results in creatine production, which is used for ATP synthesis. It was previously seen that incubation of RBCs with arginine leads to the production of citrulline, ornithine, and urea, indicating an RBC-related enzymatic machinery for arginine metabolism (42). The functional role of increased arginine catabolism may be to increase nitric oxide (NO) availability to respond to hypoxia, inducing vasodilation for an increased blood flow. Arginine supplementation increases T-cell proliferation and macrophage activity, thus it could contribute to enhance immune response (27). As well, creatine leads to ATP synthesis, which increases during the immune response to boost leukocyte proliferation and activity. Moreover, tryptophan metabolism is involved in nicotinamide and NAD production. NAD is implicated in the glycolytic pathway and oxidative phosphorylation and its formation from tryptophan metabolism was demonstrated to boost macrophage phagocytic activity during immune response (43). Dopamine has a role in the initiation of immune responses in lymphocytes (44). The biosynthesis of serotonin and dopamine, which are negatively correlated with morphological RBC deviations, is thought to decrease in COVID-19 infection due to a co-expression and a functional link with Angiotensin I Converting Enzyme 2 (ACE2) (45), the main receptor for SARS-CoV-2. Together, these data highlight the relevance of the RBC buffering effect for immune cell activity regulation. Positive correlations with plasma lactate levels are also linked to increased energy demand. Hypoxia causes a boost in glycolysis to produce and release more ATP that stimulates NO production and vasodilation, as well as 2,3-DPG that increases deoxyhemoglobin release of oxygen (34). ATP release also results in increased adenosine and xanthine in hypoxic plasma, as observed in our data. Adenosine levels remain high because PKA triggers a hypoxia-induced proteasome that degrades adenosine transporters (34), as we show from the correlation with several proteasome ATP-dependent proteins. More glycolysis results in less PPP for glutathione reduction, so less NADPH formation and presumably less antioxidant capacity of RBCs. Although the oxygen dissociation curve was not found different in COVID-19 patients (46) the presence of markers of hypoxia is expectable, considering that COVID-19 infection often results in lowered blood oxygen saturation, and in ECMO patients it is reduced until 82 % (47). A reason for no differences in the oxygen dissociation curve may be due to methemoglobin, which increases hemoglobin oxygen affinity and may compensate the opposite effect of 2,3-DPG (46). Indeed, we found positive correlations with methemoglobin and hemoglobin F globin chains, whose expression is stimulated by hypoxia (48). This highlights an effect of the infectious state also at the level of erythropoiesis.

Sphero-echinocytes show increased antioxidant activity since they are positively correlated with GSR, which catalyzes glutathione reduction, G6PD that is necessary for NADPH formation, and PRDX1, which reduces hydroperoxides. This response is associated with the infectious state since in septic patients proinflammatory cytokines such as TNF alpha promote ROS generation to destroy bacteria (40). We could not find differences in, *e.g.*, levels of band 3 (AE1), to indicate oxidative stress-associated loss of cytoskeletal proteins, but it was reported oxidation of band 3, spectrin (SPTA1) and ankyrin (ANK1) (8), which, along with alterations of the lipid compartments, may alter RBC deformability. We see that the impaired deformability in COVID-19 cells is mostly reversible, thus not indicating damaged antioxidant mechanisms in RBCs, but rather increased oxidative stress caused by higher ROS generation during the infection that may be resolved by increasing RBC antioxidant defense.

The results of our study create the basis for possible clinical impacts: convalescent plasma transfusion was shown not to be associated with improved clinical outcomes (49). While plasma transfusions from healthy individuals may benefit RBC flow properties in COVID-19 patients that may potentially decrease RBC-related thrombotic risk (50), patient antibodies would be diluted, possibly compromising the efficacy of the

medRxiv preprint doi: https://doi.org/10.1101/2022.03.31.22273226; this version posted March 31, 2022. The copyright holder for this preprint (which was not certified by peer review) is the author/funder, who has granted medRxiv a license to display the preprint in perpetuity. It is made available under a CC-BY-NC-ND 4.0 International license .

immune response to the virus. Further studies are necessary to evaluate the role of RBCs in re-establishing plasma equilibria, potentially decreasing patient mortality risk.

AUTHOR CONTRIBUTIONS

SR, GS, LK, SQ designed the study; SR, GS, ML, FG, MD, AD, SQ performed experiments and data analyses; SR and GS wrote the manuscript; AD and SQ supervised research and manuscript writing; PM and KZ provided blood samples and clinical data interpretation; CW and AD provided resources and materials. All authors revised and approved the manuscript.

ACKNOWLEDGMENTS

This work was supported by the European Union's Horizon 2020 research and innovation program under the Marie Skłodowska-Curie grant agreement No 860436 – EVIDENCE and by the Deutsche Forschungsgemeinschaft DFG in the framework of the research unit FOR 2688 'Instabilities, Bifurcations and Migration in Pulsatile Flows' WA 1336/13-1. We would like to thank Annett Wilken-Schmitz for the organizational support and collection of blood samples.

REFERENCES

1. Wu, F., S. Zhao, B. Yu, Y.-M. Chen, W. Wang, Z.-G. Song, Y. Hu, Z.-W. Tao, J.-H. Tian, Y.-Y. Pei, M.-L. Yuan, Y.-L. Zhang, F.-H. Dai, Y. Liu, Q.-M. Wang, J.-J. Zheng, L. Xu, E. C. Holmes, and Y.-Z. Zhang, 2020. A new coronavirus associated with human respiratory disease in China. *Nature* 579:265–269. http://www.nature.com/articles/s41586-020-2008-3.

2. Mehta, P., D. F. McAuley, M. Brown, E. Sanchez, R. S. Tattersall, and J. J. Manson, 2020. COVID-19: consider cytokine storm syndromes and immunosuppression. *Lancet* 395:1033–1034. http://dx.doi.org/10.1016/S0140-6736(20)30628-0.

3. Mann, E. R., M. Menon, S. B. Knight, J. E. Konkel, C. Jagger, T. N. Shaw, S. Krishnan, M. Rattray, A. Ustianowski, N. D. Bakerly, P. Dark, G. Lord, A. Simpson, T. Felton, L.-P. Ho, R. TRC, M. Feldmann, CIRCO, J. R. Grainger, and T. Hussell, 2020. Longitudinal immune profiling reveals distinct features of COVID-19 pathogenesis. *medRxiv* https://www.medrxiv.org/content/early/2020/06/16/2020.06.13.20127605.

4. Kubánková, M., B. Hohberger, J. Hoffmanns, J. Fürst, M. Herrmann, J. Guck, and M. Kräter, 2021. Physical phenotype of blood cells is altered in COVID-19. *Biophys. J.* 120:2838–2847. https://linkinghub.elsevier.com/retrieve/pii/S0006349521004549.

5. Tang, N., D. Li, X. Wang, and Z. Sun, 2020. Abnormal coagulation parameters are associated with poor prognosis in patients with novel coronavirus pneumonia. *J. Thromb. Haemost.* 18:844–847. https://doi.org/10.1111/jth.14768.

6. Varatharajah, N., and S. Rajah, 2020. Microthrombotic Complications of COVID-19 Are Likely Due to Embolism of Circulating Endothelial Derived Ultralarge Von Willebrand Factor (eULVWF) Decorated-Platelet Strings. *Fed. Pract.* 37:e1–e2. https://onlinelibrary.wiley.com/doi/10.1111/ijd.14937.

7. Della Rocca, D. G., M. Magnocavallo, C. Lavalle, J. Romero, G. B. Forleo, N. Tarantino, C. Chimenti, I. Alviz, M. T. Gamero, M. J. Garcia, L. Di Biase, and A. Natale, 2021. Evidence of systemic endothelial injury and microthrombosis in hospitalized COVID-19 patients at different stages of the disease. *J. Thromb. Thrombolysis* 51:571–576. https://doi.org/10.1007/s11239-020-02330-1.

8. Thomas, T., D. Stefanoni, M. Dzieciatkowska, A. Issaian, T. Nemkov, R. C. Hill, R. O. Francis, K. E. Hudson, P. W. Buehler, J. C. Zimring, E. A. Hod, K. C. Hansen, S. L. Spitalnik, and A. D'Alessandro, 2020. Evidence of Structural Protein Damage and Membrane Lipid Remodeling in Red Blood Cells from COVID-19 Patients. *J. Proteome Res.* 19:4455–4469. https://pubs.acs.org/doi/10.1021/acs.jproteome.0c00606.

9. D'Alessandro, A., T. Thomas, M. Dzieciatkowska, R. C. Hill, R. O. Francis, K. E. Hudson, J. C. Zimring, E. A. Hod, S. L. Spitalnik, and K. C. Hansen, 2020. Serum Proteomics in COVID-19 Patients: Altered Coagulation and Complement Status as a Function of IL-6 Level. *J. Proteome Res.* 19:4417–4427. https://pubs.acs.org/doi/10.1021/acs.jproteome.0c00365.

10. Renoux, C., R. Fort, E. Nader, C. Boisson, P. Joly, E. Stauffer, M. Robert, S. Girard, A. Cibiel, A. Gauthier, et al., 2021. Impact of COVID-19 on red blood cell rheology. *British journal of haematology* 192:e108–e111. https://pubmed.ncbi.nlm.nih.gov/33410504/.

11. Lipowsky, H. H., 2005. Microvascular Rheology and Hemodynamics. *Microcirculation* 12:5–15. http://doi.wiley.com/10.1080/10739680590894966.

12. Matthews, K., M.-E. Myrand-Lapierre, R. R. Ang, S. P. Duffy, M. D. Scott, and H. Ma, 2015. Microfluidic deformability analysis of the red cell storage lesion. *Journal of Biomechanics* 48:4065–4072. https://www.sciencedirect.com/science/article/pii/S0021929015005485.

13. Lanotte, L., J. Mauer, S. Mendez, D. A. Fedosov, J.-M. M. Fromental, V. Claveria, F. Nicoud, G. Gompper, M. Abkarian, J. Mauer, D. A. Fedosov, G. Gompper, S. Mendez, F. Nicoud, and J.-M. M. Fromental,

medRxiv preprint doi: https://doi.org/10.1101/2022.03.31.22273226; this version posted March 31, 2022. The copyright holder for this preprint (which was not certified by peer review) is the author/funder, who has granted medRxiv a license to display the preprint in perpetuity. It is made available under a CC-BY-NC-ND 4.0 International license .

2016. Correction for Lanotte et al., Red cells' dynamic morphologies govern blood shear thinning under microcirculatory flow conditions. *Proc. Natl. Acad. Sci.* 113:E8207–E8207. http://www.pnas.org/lookup/doi/10.1073/pnas.1618852114.

14. Di Carlo, D., 2012. A Mechanical Biomarker of Cell State in Medicine. *J. Lab. Autom.* 17:32–42. http://journals.sagepub.com/doi/10.1177/2211068211431630.

15. Piety, N. Z., J. Stutz, N. Yilmaz, H. Xia, T. Yoshida, and S. S. Shevkoplyas, 2021. Microfluidic capillary networks are more sensitive than ektacytometry to the decline of red blood cell deformability induced by storage. *Sci. Rep.* 11:604. https://doi.org/10.1038/s41598-020-79710-3.

16. Guckenberger, A., A. Kihm, T. John, C. Wagner, and S. Gekle, 2018. Numerical–experimental observation of shape bistability of red blood cells flowing in a microchannel. *Soft Matter* 14:2032–2043. http://xlink.rsc.org/?DOI=C7SM02272G.

17. Recktenwald, S. M., K. Graessel, F. M. Maurer, T. John, S. Gekle, and C. Wagner, 2022. Red blood cell shape transitions and dynamics in time-dependent capillary flows. *Biophys. J.* 121:23–36. https://doi.org/10.1016/j.bpj.2021.12.009.

18. Kihm, A., L. Kaestner, C. Wagner, and S. Quint, 2018. Classification of red blood cell shapes in flow using outlier tolerant machine learning. *PLOS Comput. Biol.* 14:e1006278. https://dx.plos.org/10.1371/journal.pcbi.1006278.

19. Pries, A. R., and T. W. Secomb, 2008. Blood Flow in Microvascular Networks. *In* Microcirculation, Elsevier, 3–36. https://linkinghub.elsevier.com/retrieve/pii/B9780123745309000012.

20. Secomb, T. W., 2017. Blood Flow in the Microcirculation. *Annu. Rev. Fluid Mech.* 49:443–461. http://www.annualreviews.org/doi/10.1146/annurev-fluid-010816-060302.

21. Burnum-Johnson, K. E., J. E. Kyle, A. J. Eisfeld, C. P. Casey, K. G. Stratton, J. F. Gonzalez, F. Habyarimana, N. M. Negretti, A. C. Sims, S. Chauhan, et al., 2017. MPLEx: a method for simultaneous pathogen inactivation and extraction of samples for multi-omics profiling. *Analyst* 142:442–448. https://doi.org/10.1039/C6AN02486F.

22. D'Alessandro, A., X. Fu, T. Kanias, J. A. Reisz, R. Culp-Hill, Y. Guo, M. T. Gladwin, G. Page, S. Kleinman, M. Lanteri, et al., 2021. Donor sex, age and ethnicity impact stored red blood cell antioxidant metabolism through mechanisms in part explained by glucose 6-phosphate dehydrogenase levels and activity. *Haematologica* 106:1290. https://www.ncbi.nlm.nih.gov/pmc/articles/PMC8094095/.

23. Nemkov, T., J. A. Reisz, S. Gehrke, K. C. Hansen, and A. D'Alessandro, 2019. High-throughput metabolomics: isocratic and gradient mass spectrometry-based methods. *In* High-throughput metabolomics, Springer, 13–26. https://pubmed.ncbi.nlm.nih.gov/31119654/.

24. Issaian, A., A. Hay, M. Dzieciatkowska, D. Roberti, S. Perrotta, Z. Darula, J. Redzic, M. P. Busch, G. P. Page, S. C. Rogers, et al., 2021. The interactome of the N-terminus of band 3 regulates red blood cell metabolism and storage quality. *haematologica* 106:2971. https://www.ncbi.nlm.nih.gov/pmc/articles/PMC8561282/.

25. Lim H. W., G., M. Wortis, and R. Mukhopadhyay, 2009. Red Blood Cell Shapes and Shape Transformations: Newtonian Mechanics of a Composite Membrane: Sections 2.5–2.8, Wiley-VCH Verlag GmbH & Co. KGaA, 139–204.

26. Bernhardt, I., and J. C. Ellory, 2013. Red cell membrane transport in health and disease. Springer Science & Business Media.

27. D'Alessandro, A., T. Thomas, I. J. Akpan, J. A. Reisz, F. I. Cendali, F. Gamboni, T. Nemkov, K. Thangaraju, U. Katneni, K. Tanaka, et al., 2021. Biological and Clinical Factors contributing to the Metabolic Heterogeneity of Hospitalized Patients with and without COVID-19. *Cells* 10:2293. https://pubmed.ncbi.nlm.nih.gov/34571942/.

28. Violi, F., G. Ceccarelli, L. Loffredo, F. Alessandri, F. Cipollone, D. D'ardes, G. D'Ettorre, P. Pignatelli, M. Venditti, C. M. Mastroianni, et al., 2021. Albumin supplementation dampens hypercoagulability in COVID-19: a preliminary report. *Thrombosis and Haemostasis* 121:102–105. https://www.thieme-connect.de/products/ejournals/abstract/10.1055/s-0040-1721486.

29. Claise, C., J. Saleh, M. Rezek, S. Vaulont, C. Peyssonnaux, and M. Edeas, 2022. Low transferrin levels predict heightened inflammation in patients with COVID-19: New insights. *International Journal of Infectious Diseases* 116:74–79. https://doi.org/10.1016/j.ijid.2021.12.340.

30. Messner, C. B., V. Demichev, D. Wendisch, L. Michalick, M. White, A. Freiwald, K. Textoris-Taube, S. I. Vernardis, A.-S. Egger, M. Kreidl, et al., 2020. Ultra-high-throughput clinical proteomics reveals classifiers of COVID-19 infection. *Cell systems* 11:11–24. https://doi.org/10.1016/j.cels.2020.05.012.

medRxiv preprint doi: https://doi.org/10.1101/2022.03.31.22273226; this version posted March 31, 2022. The copyright holder for this preprint (which was not certified by peer review) is the author/funder, who has granted medRxiv a license to display the preprint in perpetuity. It is made available under a CC-BY-NC-ND 4.0 International license .

31. Thomas, T., D. Stefanoni, J. A. Reisz, T. Nemkov, L. Bertolone, R. O. Francis, K. E. Hudson, J. C. Zimring, K. C. Hansen, E. A. Hod, S. L. Spitalnik, and A. D'Alessandro, 2020. COVID-19 infection alters kynurenine and fatty acid metabolism, correlating with IL-6 levels and renal status. *JCI Insight* 5:1–16. https://insight.jci.org/articles/view/140327.

32. Mangge, H., M. Herrmann, A. Meinitzer, S. Pailer, P. Curcic, Z. Sloup, M. Holter, and F. Prüller, 2021. Increased Kynurenine Indicates a Fatal Course of COVID-19. *Antioxidants* 10:1960. https://www.mdpi.com/2076-3921/10/12/1960.

33. Saliba, K. J., I. Ferru, and K. Kirk, 2005. Provitamin B_5 (Pantothenol) Inhibits Growth of the Intraerythrocytic Malaria Parasite. *Antimicrobial Agents and Chemotherapy* 49:632–637. https://journals.asm.org/doi/abs/10.1128/AAC.49.2.632-637.2005.

34. Nemkov, T., J. A. Reisz, Y. Xia, J. C. Zimring, and A. D'Alessandro, 2018. Red blood cells as an organ? How deep omics characterization of the most abundant cell in the human body highlights other systemic metabolic functions beyond oxygen transport. *Expert review of proteomics* 15:855–864. https://doi.org/10.1080/14789450.2018.1531710.

35. Conneely, O. M., 2001. Antiinflammatory activities of lactoferrin. *Journal of the American College of Nutrition* 20:389S–395S. https://doi.org/10.1080/07315724.2001.10719173.

36. Bownik, A., and Z. Stępniewska, 2016. Ectoine as a promising protective agent in humans and animals. *Arhiv za higijenu rada i toksikologiju* 67:260–264. https://doi.org/10.1515/aiht-2016-67-2837.

37. Kaur, G., X. Ji, and I. Rahman, 2021. SARS-CoV2 Infection Alters Tryptophan Catabolism and Phospholipid Metabolism. *Metabolites* 11:659. https://doi.org/10.3390/metabo11100659.

38. Burke, A. M., D. O. Quest, S. Chien, and C. Cerri, 1981. The effects of mannitol on blood viscosity. *Journal of neurosurgery* 55:550–553. https://doi.org/10.3171/jns.1981.55.4.0550.

39. Reinhart, W. H., N. Z. Piety, J. W. Deuel, A. Makhro, T. Schulzki, N. Bogdanov, J. S. Goede, A. Bogdanova, R. Abidi, and S. S. Shevkoplyas, 2015. Washing stored red blood cells in an albumin solution improves their morphologic and hemorheologic properties. *Transfusion* 55:1872–1881. https://doi.org/10.1111/trf.13052.

40. Bateman, R. M., M. D. Sharpe, M. Singer, and C. G. Ellis, 2017. The effect of sepsis on the erythrocyte. *International journal of molecular sciences* 18:1932. https://doi.org/10.3390/ijms18091932.

41. Galbraith, M. D., K. T. Kinning, K. D. Sullivan, P. Araya, K. P. Smith, R. E. Granrath, J. R. Shaw, R. Baxter, K. R. Jordan, S. Russell, et al., 2022. Specialized interferon action in COVID-19. *Proceedings of the National Academy of Sciences* 119:e2116730119. https://www.pnas.org/doi/full/10.1073/pnas.2116730119.

42. Ramírez-Zamora, S., M. L. Méndez-Rodríguez, M. Olguín-Martínez, L. Sanchez-Sevilla, M. Quintana-Quintana, N. García-García, and R. Hernandez-Munoz, 2013. Increased erythrocytes by-products of arginine catabolism are associated with hyperglycemia and could be involved in the pathogenesis of type 2 diabetes mellitus. *PLoS One* 8:e66823. https://doi.org/10.1371/journal.pone.0066823.

43. Minhas, P. S., L. Liu, P. K. Moon, A. U. Joshi, C. Dove, S. Mhatre, K. Contrepois, Q. Wang, B. A. Lee, M. Coronado, et al., 2019. Macrophage de novo NAD+ synthesis specifies immune function in aging and inflammation. *Nature immunology* 20:50–63. https://doi.org/10.1038/s41590-018-0255-3.

44. R Buttarelli, F., A. Fanciulli, C. Pellicano, and F. E Pontieri, 2011. The dopaminergic system in peripheral blood lymphocytes: from physiology to pharmacology and potential applications to neuropsychiatric disorders. *Current Neuropharmacology* 9:278–288. https://doi.org/10.2174/157015911795596612.

45. Nataf, S., 2020. An alteration of the dopamine synthetic pathway is possibly involved in the pathophysiology of COVID-19. *Journal of medical virology* 92:1743–1744. https://www.ncbi.nlm.nih.gov/pmc/articles/PMC7228370/.

46. Böning, D., W. M. Kuebler, and W. Bloch, 2021. The oxygen dissociation curve of blood in COVID-19. *American Journal of Physiology-Lung Cellular and Molecular Physiology* https://doi.org/10.1152/ajplung.00079.2021.

47. Schmidt, M., G. Tachon, C. Devilliers, G. Muller, G. Hekimian, N. Bréchot, S. Merceron, C. E. Luyt, J.-L. Trouillet, J. Chastre, et al., 2013. Blood oxygenation and decarboxylation determinants during venovenous ECMO for respiratory failure in adults. *Intensive care medicine* 39:838–846. https://doi.org/10.1007/s00134-012-2785-8.

48. Simionato, G., A. Rabe, J. S. Gallego-Murillo, C. van der Zwaan, A. J. Hoogendijk, M. van den Biggelaar, G. Minetti, A. Bogdanova, H. Mairbäurl, C. Wagner, L. Kaestner, and E. van den Akker, 2022. In Vitro Erythropoiesis at Different pO2 Induces Adaptations That Are Independent of Prior Systemic Exposure to Hypoxia. *cells* 11:1082. https://www.mdpi.com/2073-4409/11/7/1082#cite.

medRxiv preprint doi: https://doi.org/10.1101/2022.03.31.22273226; this version posted March 31, 2022. The copyright holder for this preprint (which was not certified by peer review) is the author/funder, who has granted medRxiv a license to display the preprint in perpetuity. It is made available under a CC-BY-NC-ND 4.0 International license .

49. Janiaud, P., C. Axfors, A. M. Schmitt, V. Gloy, F. Ebrahimi, M. Hepprich, E. R. Smith, N. A. Haber, N. Khanna, D. Moher, et al., 2021. Association of convalescent plasma treatment with clinical outcomes in patients with COVID-19: a systematic review and meta-analysis. *Jama* 325:1185–1195. https://jamanetwork.com/journals/jamanetworkopen/article-abstract/2788377.

50. Byrnes, J. R., and A. S. Wolberg, 2017. Red blood cells in thrombosis. *Blood, The Journal of the American Society of Hematology* 130:1795–1799. https://doi.org/10.1182/blood-2017-03-745349.